J. Fluid Mech. (2006), *vol.* 554, *pp.* 521–542.
doi:10.1017/S0022112006008871 Printed in the United Kingdom

Large-scale and very-large-scale motions in turbulent pipe flow

By M. GUALA†, S. E. HOMMEMA‡ AND R. J. ADRIAN¶

Laboratory for Turbulence and Complex Flow, Department of Theoretical and Applied Mechanics, University of Illinois, Urbana, IL 61801, USA

(Received 7 July 2005 and in revised form 21 December 2005)

In the outer region of fully developed turbulent pipe flow very large-scale motions reach wavelengths more than $8R$–$16R$ long (where R is the pipe radius), and large-scale motions with wavelengths of $2R$–$3R$ occur throughout the layer. The very-large-scale motions are energetic, typically containing half of the turbulent kinetic energy of the streamwise component, and they are unexpectedly active, typically containing more than half of the Reynolds shear stress. The spectra of the y-derivatives of the Reynolds shear stress show that the very-large-scale motions contribute about the same amount to the net Reynolds shear force, $\mathrm{d}\overline{-u'v'}/\mathrm{d}y$, as the combination of all smaller motions, including the large-scale motions and the main turbulent motions. The main turbulent motions, defined as the motions small enough to be in a statistical equilibrium (and hence smaller than the large-scale motions) contribute relatively little to the Reynolds shear stress, but they constitute over half of the net Reynolds shear force.

1. Introduction

One of the most fundamental and important characteristics of wall turbulence is its strong inhomogeneity in length scales, ranging from the viscous length scales, $\delta_\nu = \nu/u_\tau$ at the wall, to the thickness of the wall layer, δ (which will be used to represent the boundary thickness, δ, the pipe radius, R, or the channel half-height, h). While the streaky structures at the wall have spacing approximately $\sim 100\delta_\nu$, on average, they are also very long, often exceeding thousands of viscous length scales. In the outer region the 'large-scale motions' (abbreviated to LSM and sometimes called 'δ-scale motions') are known to take the form of turbulent bulges (Laufer & Narayanan 1971) whose mean height is $\sim \delta$, mean streamwise length is $\sim 2\delta$, and mean spanwise width is $\sim 1\delta$–1.5δ (Kovasznay, Kibens & Blackwelder 1970; Brown & Thomas 1977; Cantwell 1981; Murlis, Tsai & Bradshaw 1982). The Kármán number $\delta^+ = \delta/\delta_\nu$ characterizes the ratio of the δ-scale motions to the near-wall motions. It is also equal to the turbulent Reynolds number, $Re_\tau = u_\tau\delta/\nu$, and since Re_τ must be large for turbulent flow, the range of scales is necessarily large.

In their pioneering studies, Townsend (1958) and Grant (1958) observed long tails in the time-delayed auto-correlation functions of the streamwise velocity, u, that were non-zero out to lengths as long as 1.4δ. They rightly inferred that large-scale

† Present address: Institute for Hydromechanics and Water Res. Man., ETH Zurich, Switzerland.
‡ Present address: ExxonMobil Upstream Research Co., PO Box 2189, Houston, TX 77252, USA.
¶ Present address: Mechanical and Aerospace Engineering Department, Arizona State University, Tempe, AZ 85287 USA.

motions existed, even close to the wall, and that they carried a significant fraction of the turbulent kinetic energy. Various correlation studies (Favre, Gaviglio & Dumas 1967; Bradshaw 1967; Tritton 1967; Blackwelder & Kovasznay 1972) supported and amplified their observations concerning the energy of the streamwise component in what have become known as Townsend's 'large eddies'. Spectral studies provide a more incisive evaluation of the distribution of energy in the large scales. Bullock, Cooper & Abernathy (1978) convincingly showed that the energy contained in the low-wavenumber (denoted by k_x) region of the streamwise velocity spectrum was far from being negligible. At the high-wavenumber end of the k_x^{-1} range, they found a peak in the pre-multiplied longitudinal spectrum that was located at a streamwise wavelength $\lambda_x^+ \sim 600$ in the buffer layer (superscript $^+$ denotes non-dimensionalization by the viscous scales) and grew to $\lambda_x \sim R$ above $y/R \sim 0.6$. Similar behaviour can be seen in the spectra presented in Perry & Abell (1975). Perry, Henbest & Chong (1986) found the that location of the corresponding spectral peak increased as $\lambda_x \sim 5y$ between $y^+ = 100$ and $y/R = 0.3$ and reached a value of $\lambda_x \sim 3R$ at greater distances from the wall. In each case the area under the peaks indicated significant energy content.

The turbulent bulges or 'large-scale motions' (LSMs) have often been interpreted to account for the long correlation tails and the spectral peaks at the high-wavenumber end of the k_x^{-1} range, and therefore to be the 'large eddies' discussed by Townsend (1961, 1976). Studies of the mean time between turbulent bursts, T, also associate the bursting phenomena with a length scale of the order of the mean bulge length. Laufer & Narayanan (1971) proposed outer scaling for the mean time, and they found a value of $U_\infty T/\delta = 5$ that was substantially independent of the Reynolds number (U_∞ is the free-stream velocity). The review by Bandyopadhyay (1982) concludes that $2.5 < U_\infty T/\delta < 10$, while the review by Fleischmann & Wallace (1984) used scaling with the local mean velocity to reduce the spread to $1.5 < U_\infty T/\delta < 3.5$, very close to the mean length of a turbulent bulge. Also, see the discussion of LSMs in Falco (1991).

Fleischmann & Wallace (1984) also associated the large-scale motions in bounded flows such as in pipes and channels with those in the turbulent boundary layer. Using proper orthogonal decomposition (POD) on a domain $2.4h$ long in channel flow to evaluate the energy distribution associated with two-dimensional patterns in the streamwise-wall-normal plane, Liu, Adrian & Hanratty (2001) found over half of the layer-averaged kinetic energy residing in the lowest-order modes. The 12 most energetic modes had streamwise wavelengths of infinity, $2.4h$ and $1.2h$, and heights of h and roughly $h/2$ (the POD could not distinguish between the modes of length $2.4h$ and the longer modes that were aliased into the domain $2.4h$ long). Thus, the energetic modes are not only long but also tall. That is they are large in y as well as x. In addition to the large-scale motions of order δ, there is also substantial evidence for the existence of very large scales with lengths ranging up to 10δ–50δ, containing a significant fraction of the total kinetic energy (Priymak & Miyazaki 1994; Hites 1997; Jiménez 1998; Kim & Adrian 1999, hereafter referred to as KA99; Hunt & Morrison 2000). These 'very-large-scale motions' (VLSM) or 'super-δ scale' motions are by definition motions that are longer than the mean bulge length. Jiménez (1998) and KA99 both report scales as large as 14δ–20δ, based on examination of various experimental spectra.

A representative power spectrum of streamwise velocity in turbulent pipe flow is shown in figure 1(a). Lines indicating -1 and $-5/3$ power laws are shown for reference. The same spectrum multiplied by k_x and plotted on semi-logarithmic axes

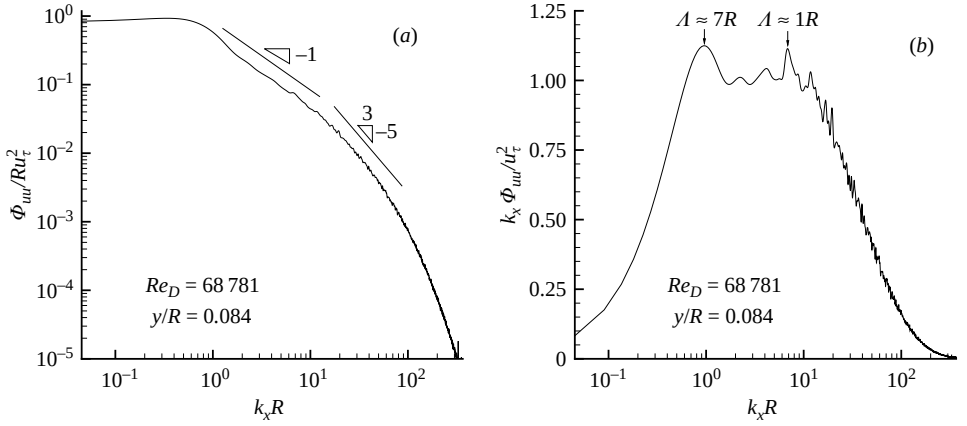

FIGURE 1. (*a*) Power spectrum of streamwise velocity fluctuation. (*b*) Pre-multiplied power spectrum of streamwise velocity fluctuation. In (*b*) two peaks in the spectrum are observed with corresponding streamwise wavelengths of approximately $7R$ and $1R$, respectively. (Data acquired as part of the current study, following KA99).

is given in figure 1(*b*). When plotted in this manner, equal areas under the curve represent equal energies. The pre-multiplied spectrum has an appearance very similar to those found in Perry & Abell (1975) and earlier studies. Jiménez (1998) used plots of this type to identify the beginning and end of the k_x^{-1} range, and he associated the beginning of the range with the very large scales. KA99 interpreted the shape of the premultiplied spectra as indicating a bi-modal distribution with the wavelengths at which the maxima occur representing the very-large-scale motions and the large-scale motions, respectively. Both studies concluded that the streamwise energetic modes in turbulent pipe flow have wavelengths that range between 2 and 12–14 pipe radii, depending mainly on wall-normal location. Hites (1997) found a somewhat shorter wavelength from the maximum in his pre-multiplied spectrum, $\lambda_x \sim 4\delta$, but Jiménez (1998) argues that this is due to inadequately long time series distorting the low-frequency spectrum.

Unfortunately, for almost two decades very large-scale motions have been almost neglected, despite the availability of clear evidence regarding their significance. One source of confusion was that there was no commonly accepted definition of large and very-large-scale motions, nor of turbulent bulges. Therefore a quantitative evaluation of the energy and the Reynolds stress associated with each scale has not been clearly established. Indeed, as noted above, the turbulent bulges or 'large-scale motions' have often been interpreted as accounting for the long correlation tails and therefore to be the 'large eddies' discussed by Townsend (1976), with no further distinction from the VLSM. Only in the last few years have experimental, numerical and theoretical studies begun to clarify the distinction between these two scales of motion.

For the purposes of present discussion, the wavenumber $k_xR = 2$ will be taken as the dividing line between the range of VLSM wavenumbers and the range of LSM wavenumbers. This corresponds to a wavelength of πR, which is slightly longer than the accepted mean bulge length. This choice is nominal, and the reader might feel that the value $k_xR = 1$ lies closer to the middle of the wavenumber range separating the LSM peak and the VLSM peak. However, we shall see later, in conjunction of the discussion of the net force spectra in figure 9, that $k_xR = 2$ is a slightly better motivated nominal boundary.

Numerical studies by Priymak & Miyazaki (1994) for pipe flow with Reynolds number 4000 found the most energetic mode at $y^+ = 3$ to have wavelength $\sim 25R$. However, in these studies the Kármán number is only 150, and the flow is close to transition, making interpretation with respect to fully turbulent flow problematic. Numerical experiments to study large eddies in relatively long channel flow boxes ($8\pi\delta$) at fully turbulent Reynolds numbers have been conducted recently by Jiménez, DelAlamo & Flores (2004) and del Alamo *et al.* (2004). The former concentrated on the near-wall layer and the latter concentrated on the outer layer. Super-δ-scale motions were found in both regions of the long simulation. These studies have been valuable in providing scaling for the k_x, k_z spectra and evidence for different behaviour distinguishing the LSMs and VLSMs.

While there is reasonable agreement on the contribution of large-scale motions to the turbulent kinetic energy, it is still not entirely clear where and how much those structures contribute to the Reynolds shear stresses. Originally, Townsend inferred that large-scale structures in the near-wall region are not 'active', in the sense that they do not significantly contribute to the Reynolds stress. However, pre-multiplied u, v co-spectra in Krogstad, Antonia & Browne (1992) reveal non-negligible energy distributions in the low-wavenumber regions, which was also observed in Bradshaw (1967), who suggested that the activity should extend into the logarithmic layer. Even as early as 1970 the work of Lawn (1971) found non-negligible u, v co-spectral density out to 50δ and Blackwelder & Kovasznay (1972) asserted that "the 'large eddies' contribute at least 50 % to the turbulent energy ... and about 80 % to the Reynolds stress" at locations in the outer layer.

Liu *et al.* (2001) report that the 12 POD modes containing half of the kinetic energy contain two-thirds to three-quarters of the Reynolds shear stress in the outer region. Jimenez *et al.* (2004) found that, in the near-wall region, structures longer than twice the production peak contain more than 50 % of the energy of both the streamwise velocity component and of the Reynolds stresses. According to KA99, and consistent with the observations of Perry & Abell (1975) and Bullock *et al.* (1978), the contribution to the streamwise velocity component in the outer layer should increase towards larger scales, with a peak located roughly at $y/R = 0.25 \simeq 0.3$. Results from del Alamo *et al.* (2004) at $Re_\tau = 934$ indicate that at one-third of the channel height h, structures larger than $20h$ still contribute to the Reynolds stresses.

It is clear that large-scale and very-large-scale structures are quite important with respect to turbulent quantities such as kinetic energy and Reynolds shear stress, but that many questions remain open. This work focuses on determining the contribution of large-scale and very-large-scale motions to the kinetic energy and most importantly to the Reynolds shear stress in the outer region of turbulent pipe flow. This will be done by co-spectral analysis using very long records to capture the largest scales of motion. The primary purpose is to determine the role the large-scale motions play in the mean momentum budget as a function of location in the turbulent layer. To this end we will also attempt to evaluate the y-derivative of the co-spectra to determine if the variation of such large scales can be sufficient to produce a net Reynolds force in the mean momentum budget.

2. Experimental apparatus

The experiments were performed in a fully developed 127 mm diameter turbulent pipe flow similar to that used by KA99 and Lekakis (1988). The flow apparatus consisted of an axial flow blower, appropriate flow conditioning sections, and a

Data set	Re_τ	Re_D	U_{CL} [m s^{-1}]	u_τ [m s^{-1}]	δ_ν [μm]
I	3815	192 700	22.76	0.99	15.17
II	5884	318 900	37.67	1.39	10.79
III	7959	422 300	49.89	1.86	7.98

TABLE 1. Summary of experimental data sets used in spectral computations. ($Re_\tau = u_\tau R/\nu$; $Re_D = U_{CL} D/\nu$; U_{CL}: centreline velocity; u_τ: friction velocity; δ_ν: viscous length scale.)

127 mm diameter Plexiglas pipe whose total length-to-diameter ratio was $L/D = 120$. The air velocity at the centreline of the pipe could be varied up to 50 m s^{-1}. Velocity profiles, single-point second-order moments and velocity spectra in this apparatus have been shown by Lekakis (1988), KA99 and Hommema (2001) to be consistent with fully developed turbulent pipe flow data of other investigators (Perry & Abell 1975; Bullock *et al.* 1978). Additional information regarding the equipment and procedures used in data acquisition is available in Hommema (2001). The viscous length scale, δ_ν, and the friction velocity, u_τ, are used for inner scaling of flow quantities. The centreline streamwise velocity, U_{CL}, and pipe radius, R, are used for outer scaling of flow quantities. The friction velocity was determined from static pressure drop measurements.

The data presented here were taken in experiments that repeated those described in Hommema (2001), except that they used a more advanced thermal anemometer and digitizer that produced more reliable cross-spectral density results. A dual-sensor hot-film anemometer system, TSI Model IFA 300 with a TSI Model 1241 X-film probe using 0.02 mm diameter cylindrical films, were used to record time records of the streamwise and wall-normal velocity. The DC-coupled analogue voltages from the hot-film sensor were low-pass filtered at 10 kHz, sampled simultaneously at 20 kHz and stored in records that were 32 768 (2^{15}) points long, spanning at least 1.6 s of real time. The number of such records for each experimental condition varied from 100 to 300. The voltages were converted into velocity components using a cooling velocity/yaw response calibration. Turbulent fluctuations were defined as deviations from the record averaged means. Note that the time average from a single realization was used rather than an ensemble average. Even at the lowest Reynolds number, a data record of 1.6 s spanned 12.8 m. Using the average velocity from a single realization to define fluctuations ensured that long-time fluctuations associated with scales longer than the apparatus and caused by drifts in ambient conditions did not affect the results. Further discussion of the equipment and procedures used in the data acquisition is given in Hommema (2001). Three data sets are presented and their pertinent experimental parameters are summarized in table 1. Each of the three data sets contained measurements at 8 wall-normal locations in the range $0.05 < y/R < 1.0$.

3. Spectral density functions

3.1. *Frequency spectral densities and their measurement*

We denote the ith component of the turbulent fluctuating velocity by $u_i(x, y, z, t)$ where $u_1 = u$ represents the streamwise component and $u_2 = v$ represents the wall-normal component. The mean streamwise velocity is denoted by $U(y)$. We assume all signals are stationary. The time-delayed one-dimensional cross-correlation is given by

$$R_{ij}(\tau; y) = \langle u_i(x, y, t) u_j^*(x, y, t + \tau) \rangle. \tag{3.1}$$

The co-spectrum (cross power spectral density) is defined in terms of this correlation:

$$S_{ij}(\omega, y) \equiv \frac{1}{2\pi} \int_{-\infty}^{\infty} \mathrm{e}^{-\mathrm{j}\omega\tau} R_{ij}(\tau; y)\, \mathrm{d}\tau, \tag{3.2}$$

or equivalently,

$$R_{ij}(\tau; y) = \int_{-\infty}^{\infty} \mathrm{e}^{\mathrm{j}\omega\tau} S_{ij}(\omega; y)\, \mathrm{d}\omega. \tag{3.3}$$

The frequency spectral densities are estimated from a set of $M > 100$ discrete records, $u_i^{(m)}(x, y, t)$, each consisting of $N = 32\,768$ samples where $m = 1, 2, \ldots, M$; $t = t_o, t_o + \Delta t, \ldots, t_o + T$; and $\Delta t = T/N$. The discrete Fourier transform of an N-point record is given by

$$\mathscr{F}\{\cdot\} = \sum_{\alpha=0}^{N-1} (\cdot)_\alpha \, \mathrm{e}^{-\mathrm{j}2\pi m\alpha/N}. \tag{3.4}$$

Let $W(t)$ be a window function. The discrete Fourier transform of the windowed signal is given by

$$\mathscr{F}\{W u_I^{(m)}\} = \sum_{\alpha=0}^{N-1} W_\alpha u_{i\alpha}^{(m)} \, \mathrm{e}^{-\mathrm{j}2\pi m\alpha/N}. \tag{3.5}$$

A Hanning (full cosine taper) window was applied to each zero-mean time signal to suppress the Gibb's phenomenon at high frequencies. This window caused negligible distortion of the spectra because the time records were extremely long.

Estimates of the two-sided cross power spectral density were computed using these discrete Fourier transforms. Given two records u_i and u_j, and a window W, the cross power spectral density can be estimated by (Bendat & Piersol 1986)

$$\widehat{S_{ij}}(\omega) = c \left\langle \mathscr{F}\{W u_i'\} \mathscr{F}^*\{W u_j'\} \right\rangle_M, \tag{3.6}$$

where c is a constant determined by satisfying

$$\overline{u_i' u_j'} = \int_{-\infty}^{\infty} \widehat{S_{ij}}(f)\, \mathrm{d}f, \tag{3.7}$$

$\omega = 2\pi f$ and $\langle\rangle_M$ denotes the average over the ensemble of M realizations.

3.2. *Estimation of wavenumber spectra*

Using Taylor's frozen field hypothesis and a convection velocity U_c, wavenumber spectra are conventionally approximated in terms of the corresponding frequency spectra. Consider the cross-correlation with streamwise separation

$$R_{ij}(r_x; y) = \langle u_i(x, y, t) u_j(x + r_x, y, t) \rangle \tag{3.8}$$

$$= \left\langle u_i(x, y, t) u_j\left(x, y, t - \frac{r_x}{U_c}\right) \right\rangle \tag{3.9}$$

$$= R_{ij}\left(\tau = -\frac{r_x}{U_c}; y\right), \tag{3.10}$$

since $r_x = -U_c \tau$. Here, the co-spectrum is defined as

$$S_{ij}(k_x\,;y) \equiv \frac{1}{2\pi}\int_{-\infty}^{\infty} \mathrm{e}^{-\mathrm{j}k_x r_x} R_{ij}(r_x\,;y)\,\mathrm{d}r_x \tag{3.11}$$

$$= \frac{U_c}{2\pi}\int_{-\infty}^{\infty} \mathrm{e}^{\mathrm{j}k_x U_c \tau} R_{ij}(\tau\,;y)\,\mathrm{d}\tau \tag{3.12}$$

$$= U_c S_{ij}(\omega = k_x U_c). \tag{3.13}$$

In general, S_{ij} is a complex number. We will employ Taylor's hypothesis and the identity

$$S_{ij}(k) = S_{ij}^{*}(-k) \tag{3.14}$$

to convert the two-sided estimate given in (3.6) to a one-sided wavenumber co-spectrum

$$\widehat{\Phi_{ij}}(k) = \widehat{S_{ij}}(-k) + \widehat{S_{ij}}(k) = 2\ \mathrm{Re}\{\widehat{S_{ij}}(k)\}. \tag{3.15}$$

Finite-ensemble averages of $\langle\widehat{\Phi_{ij}}(k_x)\rangle_M$ with $M > 100$ are used to form the final estimates of the one-sided wavenumber spectra. For brevity we will denote $\langle\widehat{\Phi_{ij}}(k_x)\rangle_M$ by Φ_{ij}.

The approximations involved in using Taylor's hypothesis merit some discussion. First, as pointed out by KA99 and many earlier authors, Taylor's hypothesis may not be accurate for the large scales of interest here. This will not corrupt the present results unduly since we would expect the time-delayed correlation to decay faster than the two-point correlation due to the evolution of turbulent eddies as they pass over the probe. Therefore, wavenumber spectra determined from $k_x = 2\pi f/U_c(y)$ will reveal less energy at low wavenumbers than the true wavenumber spectrum. Our accounting of energy in the largest scales will be a conservative estimate. Second, we will replace the convection velocity with the local mean velocity at the wall-normal location of interest, $U_c = U(y)$. The main goal of this study is not to present accurate wavenumber spectra, but to show that a considerable fraction of the Reynolds stress, including the Reynolds shear stress, comes from the very large scales of motion. For this purpose, the errors involved with Taylor's hypothesis and the convection velocity are not large enough to affect the conclusions.

4. Contribution of large- and very-large-scale motions

The work of KA99 spanned a Reynolds number range $33\,800 < Re_D < 115\,400$ and utilized only a single hot wire. This limited their focus to Φ_{uu}. In this work, u and v time records will be used, allowing the examination of co-spectra, and the Reynolds number will be extended up to $Re_D > 422\,000$. Figure 2(*a–c*) presents the power spectra Φ_{uu}, normalized by the pipe radius and friction velocity, for three Reynolds numbers. All spectra presented here are finite-record-length estimates. As expected, a region varying approximately as ${k_x}^{-1}$ occurs at all three Reynolds numbers. Only for the highest wavenumbers are high-frequency noise and/or aliasing due to imperfect low-pass filter evident.

Analysis of the acoustic modes of the pipe indicate that the resonant frequencies can be predicted approximately by simple analytic treatments. The relative power of the acoustic resonance modes was less than 0.14 %. There was no evidence that the acoustic resonance affected the shape of the broadband spectrum. Thus, acoustic resonance had little effect on the results or conclusions presented here, except to contaminate the spectra with a narrow-band peak, in the range $10^{-1} < k_x R < 10^{0}$. After removing this peak, the spectra are generally consistent with fully

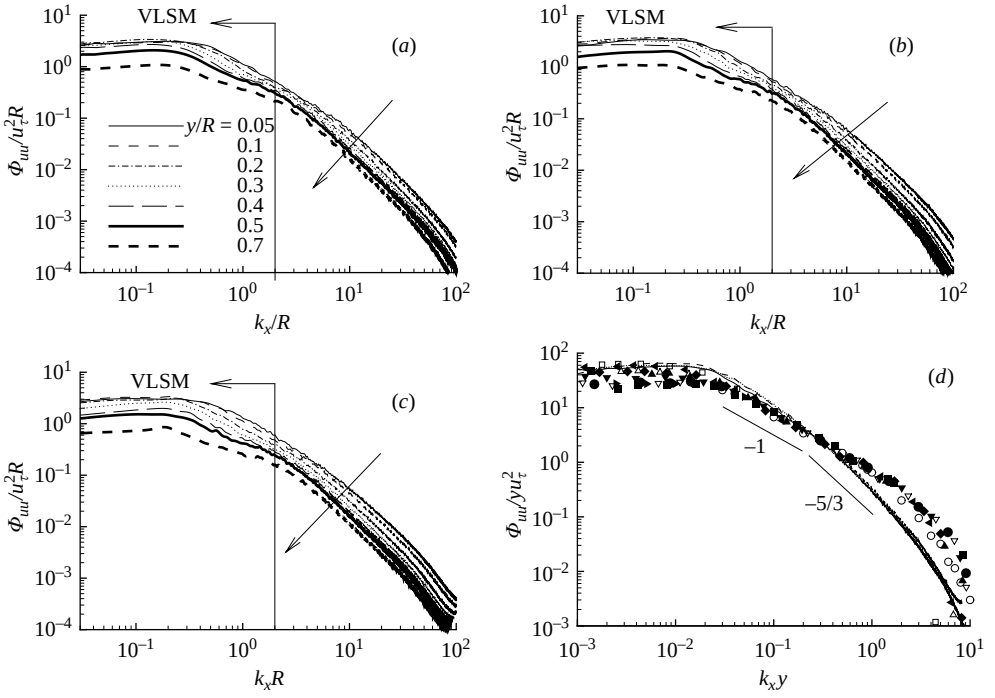

FIGURE 2. Power spectra of streamwise velocity fluctuations, Φ_{uu}, versus streamwise wavenumber, $k_x R$. (*a*) $Re_\tau = 3815$; (*b*) $Re_\tau = 5884$; (*c*) $Re_\tau = 7959$. Curves are shown for $y/R =$ 0.05, 0.1, 0.2, 0.3, 0.4, 0.5 and 0.7, increasing in the direction of the arrow. (*d*) Power spectra of streamwise velocity fluctuations, Φ_{uu}, scaled with y and u_τ, following Perry & Abell (1975). Lines are from the current study at $y/R = 0.05$ and the following three Reynolds numbers: —, $Re_\tau = 3815$; – –, $Re_\tau = 5884$; ···, $Re_\tau = 7959$. Symbols are data from Morrison *et al.* (2004): ○, $Re_\tau = 1500$, $y/R = 0.051$, and from Perry & Abell (1975): ■, $Re_\tau = 1676$, $y/R = 0.0934$; ▲, $Re_\tau = 2340$, $y/R = 0.043$; ▼, $Re_\tau = 2340$, $y/R = 0.0645$; ►, $Re_\tau = 2340$, $y/R = 0.086$; ◄, $Re_\tau = 3330$, $y/R = 0.03$; ◆, $Re_\tau = 3330$, $y/R = 0.04$; ●, $Re_\tau = 3330$, $y/R = 0.08$; □, $Re_\tau = 4810$, $y/R = 0.03$; △, $Re_\tau = 4810$, $y/R = 0.05$; ▽, $Re_\tau = 4810$, $y/R = 0.09$.

developed turbulent pipe flow spectra published by others in the wavenumber range of the acoustic modes. To demonstrate that the present data share common spectral properties with widely accepted earlier data for pipe flow, selected results from the region of the log layer are compared to the spectra of Perry & Abell (1975) and Morrison *et al.* (2004) in figure 2(*d*). This is a worst case comparison for our data, because the X-probe resolution and the sampling rate are both marginal to resolve the small scales at $y/R = 0.05$ Consequently, the spectra are attenuated at high wavenumbers.

Spectra of wall-normal velocity fluctuations are presented in figure 3. The trend with wall-normal location is similar to that reported for the streamwise velocity fluctuations, except for the 'crossing-over' observed within the range $1 < k_x R < 9$. In the low-wavenumber region the energy density increases from the wall to a wall-normal location $y/R = 0.2$–0.3, and then decreases again. In the high-wavenumber region, it always decreases. The spectra are grouped in two separate plots to make this phenomenon clearer. Lower values of the wall-normal velocity spectra relative to those of the streamwise velocity spectra reflect the difference in the total energy of these two components.

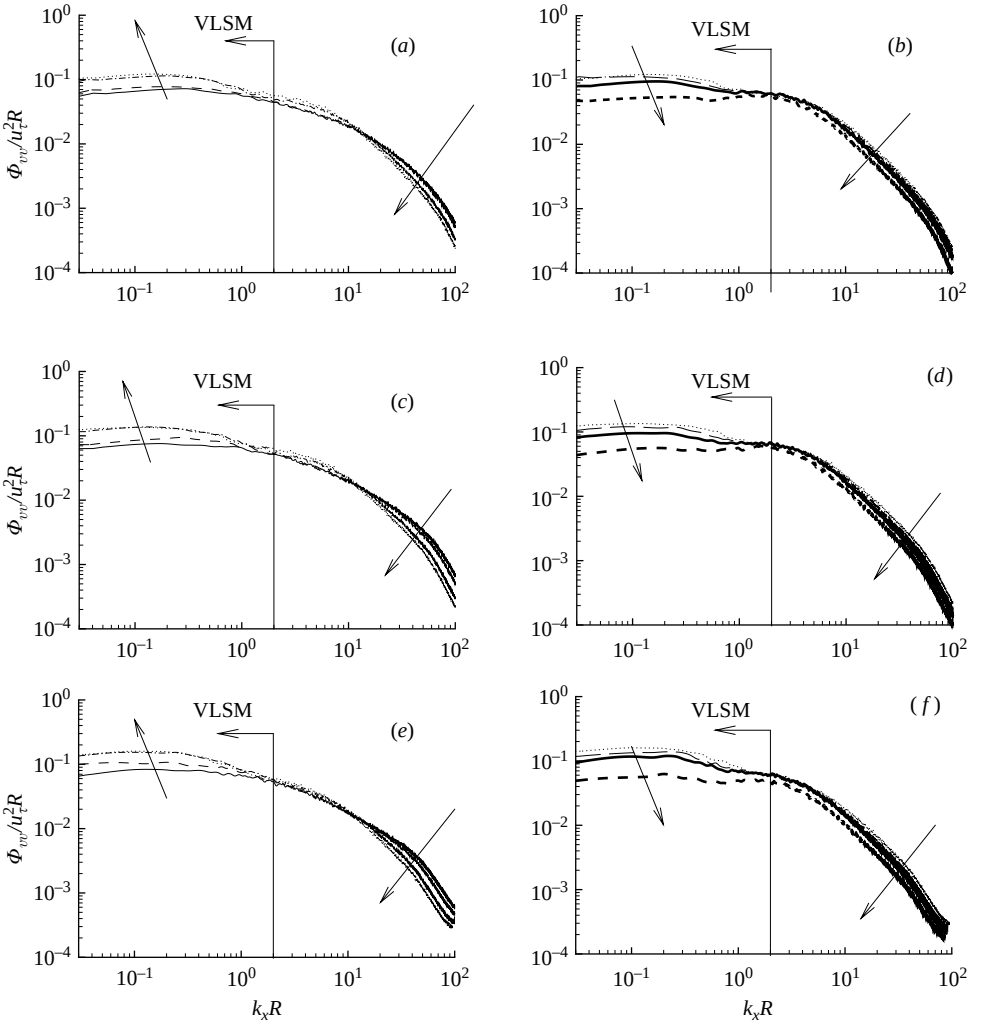

FIGURE 3. Power spectra of wall-normal velocity fluctuations, Φ_{vv}, versus streamwise wavenumber, k_x, for $Re_\tau = 3815$ (a,b), $Re_\tau = 5884$ (c,d) and $Re_\tau = 7959$ (e,f). The curves are labelled as in figure 2(a).

4.1. *Pre-multiplied spectra*

Following KA99 pre-multiplied spectra of the streamwise velocity are used to identify the wavelengths Λ_{max} associated with the large-scale structures (higher wavenumber peak) and very-large-scale structures (lower wavenumber peak). The results have been compiled in figure 4(d) with additional values of Λ_{max} extracted from other turbulent pipe flow studies, including those of Perry & Abell (1975); Bullock *et al.* (1978) and Perry *et al.* (1986). Data from the entire set of experiments are scattered, but to within experimental uncertainty the present results agree with the trends and values found in other experiments. Thus, the occurrence of large-scale and very-large-scale motions is not a facility-dependent phenomenon. Also, the trends are similar to those found in direct numerical simulations in long channels by del Alamo *et al.* (2004), providing yet more evidence for the universality of the effect. Figure 4(d) improves on the plot

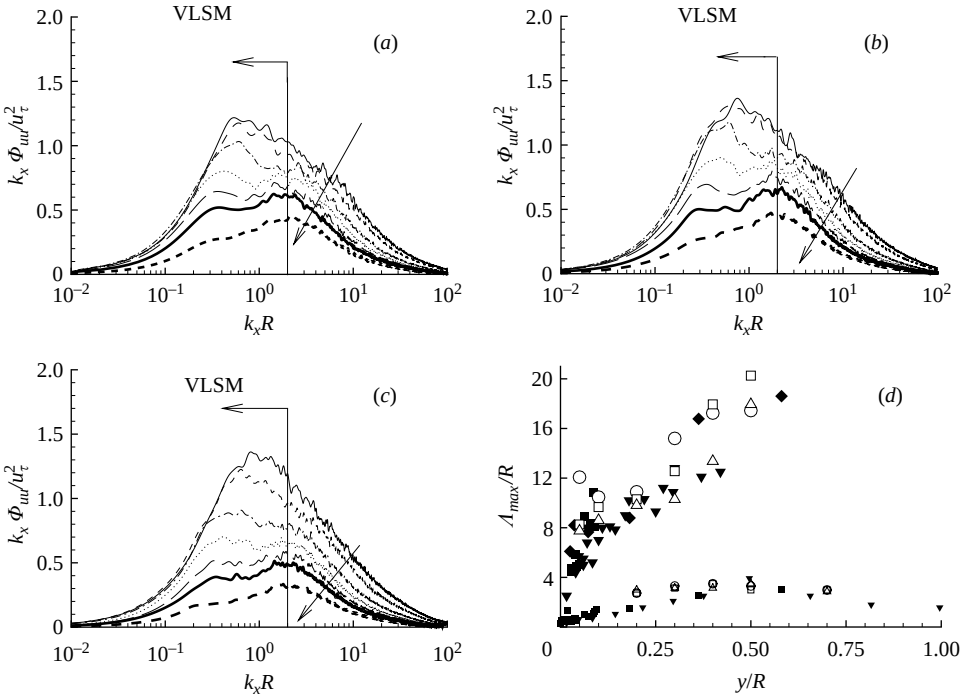

FIGURE 4. Pre-multiplied power spectra of streamwise velocity fluctuations, $k_x\Phi_{uu}$, versus streamwise wavenumber, k_x, for $Re_\tau = 3815$ (*a*), $Re_\tau = 5884$ (*b*) and $Re_\tau = 7959$ (*c*). Curves are shown for $y/R = 0.05$, 0.1, 0.2, 0.3, 0.4, 0.5 and 0.7, as in figure 2(*a*). (*d*) Wavelengths of the peaks in pre-multiplied power spectra of streamwise velocity. Large wavelengths corresponding to very-large-scale motions are shown as large symbols. Smaller wavelengths corresponding to the large-scale motions are shown as small symbols. Open symbols are from the current study, ○, $Re_\tau = 3815$; □, $Re_\tau = 5884$; △, $Re_\tau = 7959$. Closed triangles are from Kim & Adrian (1999), ▼, $Re_\tau = 3175$. Remaining closed symbols are from the literature: ■, Perry & Abell (1975); ◆, Bullock *et al.* (1978).

found in KA99 by differentiating between the higher and lower wavenumber maxima. Owing to reduced noise in the spectral measurements, these two peaks can still be resolved in areas where they appeared to merge in the KA99 spectra. Between the wall and the middle of the layer, around $y/R = 0.5$, Λ_{max}/R increases monotonically. Above $y/R = 0.5$ a lower wavenumber peak cannot be discerned. For the lowest Reynolds number, the value of Λ_{max}/R for the VLSM attains a maximum value near 12 at $y/R = 0.5$.

With increasing Re_D the value of Λ_{max}/R for the VLSMs increases slowly to about 16 at $y/R = 0.5$. The value of Λ_{max}/R for the LSMs varies much less across the layer, increasing from a small value at the wall to a maximum of about 3 near $y/R = 0.5$. KA99 suggested that the structures with wavelengths of approximately $2R$–$3R$ are associated with the organization and streamwise alignment of hairpin vortices into hairpin packets that ultimately grow to become bulges, since the mean length of the bulges is known to be of this size. The turbulent bulges found by Kovasznay *et al.* (1970) are a phenomenon of the boundary layer, but evidence found since shows that bulge-like structures also occur in pipes and channels (Fleischmann & Wallace 1984). For purposes of discussion of the wake region we decided earlier to use $k_x R = 2$, corresponding to $\lambda = \pi R$, to delimit low wavenumbers (very-large-scale motions)

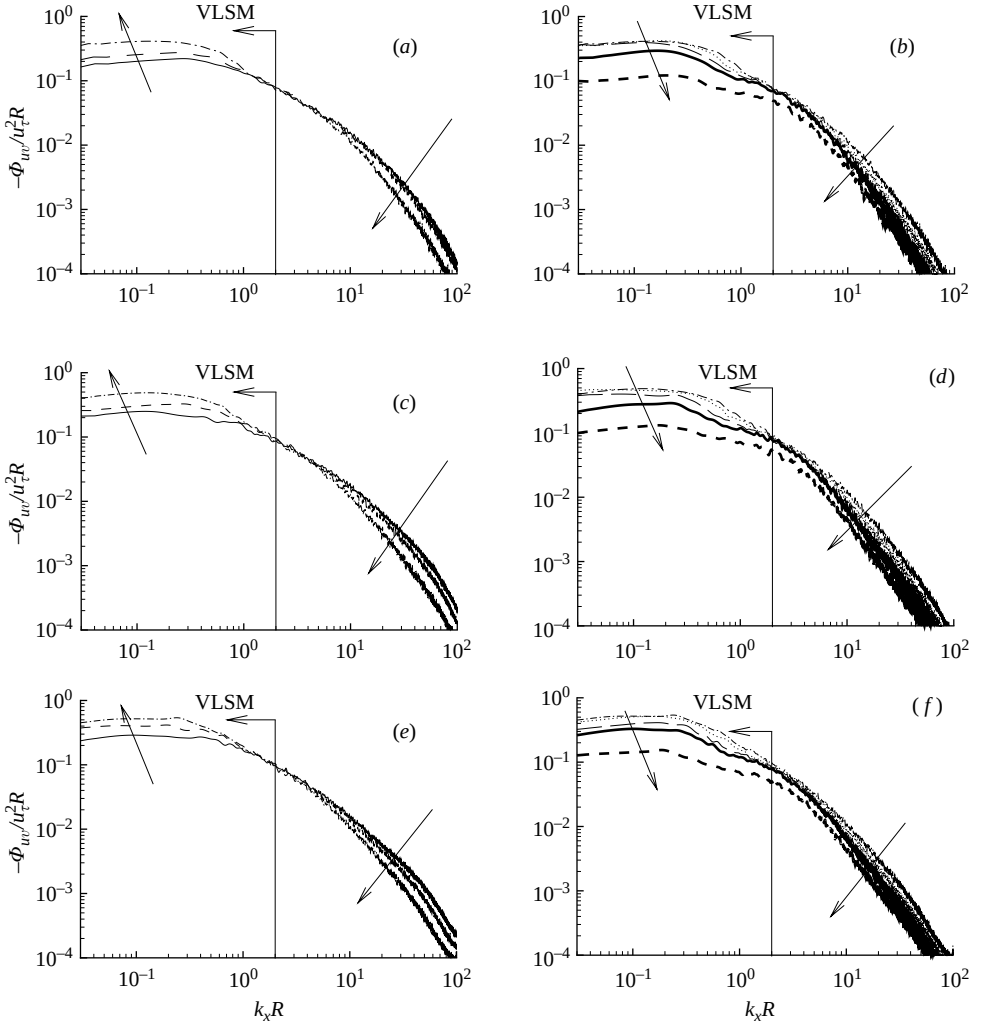

FIGURE 5. Power co-spectra of the streamwise, u, and wall-normal, v, velocity versus streamwise wavenumber, k_x, for $Re_\tau = 3815$ (a,b), $Re_\tau = 5884$ (c,d) and $Re_\tau = 7959$ (e,f). Lines are labelled as in figure 2(a).

from high wavenumbers (large-scale and smaller motions). We shall nominally take $\lambda = \pi R$ ($k_x R = 2$) to be the boundary between the large-scale motions and the main turbulent motions. The exact boundary depends on y, and it can be found by reference to the spectra.

4.2. *Velocity co-spectra*

The magnitudes of the complex co-spectra of u and v are plotted versus k_x in figure 5. Non-dimensionalization by R is used to make the y-dependence of the contributions made by the various scales more explicit. There is a clear dependence on the wall-normal location, both at high and low wavenumber. The co-spectra share many similarities with the power spectra shown earlier. Specifically, in the logarithmic layer, up to $y/R = 0.2$, they cross over around $k_x R = 2$, corresponding to the transition from large-scale to very-large-scale motion. Thus, with increasing

height in the logarithmic layer, the contribution of the very-large-scale motions increases, while the contributions of the large-scale motions and the main turbulent motions in the inertial sub-range become smaller. Above $y/R = 0.2$ the latter trend continues, and the contribution of the very large scales also decreases monotonically, as the average value of uv approaches zero at the centreline. Differences observed by varying Reynolds number are not substantial.

4.3. *Cumulative energy distribution*

One of the principal questions to be addressed in this paper is the extent to which the very-large-scale motions and the large-scale motions contribute to the kinetic energy and the Reynolds shear stress. The contribution of structures with a given range of scales (wavelengths) to the energetics of the flow is difficult to determine solely from spectral plots. Instead, we will examine the cumulative energy and Reynolds stress distribution as a function of streamwise wavenumber, or wavelength. The information is, of course, contained in the spectral plots presented above and in many earlier investigations, although the availability of u, v co-spectra with stable, well-resolved low-wavenumber ranges has been limited. The significant contribution made by very large scales and the implications of this phenomenon have not, perhaps, been fully appreciated. The cumulative contribution to $\overline{u_i u_j}$ from all wavenumbers from $k = 2\pi/\Lambda$ to infinity is

$$\Upsilon_{ij}\left(k = \frac{2\pi}{\Lambda}\right) = 1 - \frac{\displaystyle\int_0^k \Phi_{ij}(\tilde{k})\,\mathrm{d}\tilde{k}}{\displaystyle\int_0^\infty \Phi_{ij}(\tilde{k})\,\mathrm{d}\tilde{k}}, \tag{4.1}$$

where the integrals are computed numerically using discrete data,

$$\Upsilon_{ij}\left(k = \frac{2\pi}{\Lambda}\right) = 1 - \frac{\displaystyle\sum_0^k \Phi_{ij}(k)}{\displaystyle\sum_0^{k_{\max}} \Phi_{ij}(k)}. \tag{4.2}$$

Also, $\Upsilon_{ij}(\Lambda)$ is the cumulative contribution of all wavelengths from Λ to 0, and $1 - \Upsilon_{ij}(\Lambda)$ is the contribution from all wavelengths greater than Λ. Interpretation of the cumulative distributions requires some discussion of the effects of finite frequency response and spatial resolution of the X-probe. The 10 kHz frequency response was adequate to resolve streamwise scales greater than $2.27\,\mathrm{mm} = 0.0375R$, $3.76\,\mathrm{mm} = 0.0593R$ and $5\,\mathrm{mm} = 0.079R$ for the three Reynolds numbers, respectively. Scales smaller than these values were attenuated by the low-pass filter and by the less important filtering effect of the 1 mm active length of each hot film. The spectra, and therefore the cumulative distributions, under-represent the smallest scales of motion. However, our main concern is with the contributions of the large scales, and for this purpose the limited frequency response of the data is satisfactory to within an error equal to the amount the total quantity is underestimated. For the power spectra of u and v above $y/R = 0.1$ the maximum attenuation of the total is estimated to be 5–7 %, based on extrapolation to the viscous cut-off. For the Reynolds shear stress the maximum error is conservatively bounded by 10–20 % at the highest Reynolds number, and 5–10 % at the lower Reynolds number. This is based on comparison of the values for $\overline{u'v'}$ to the linear variation of total stress at $y/R = 0.1$–0.2 where viscous stresses are small. The magnitude and trend in the $\overline{u'v'}$ errors are very similar

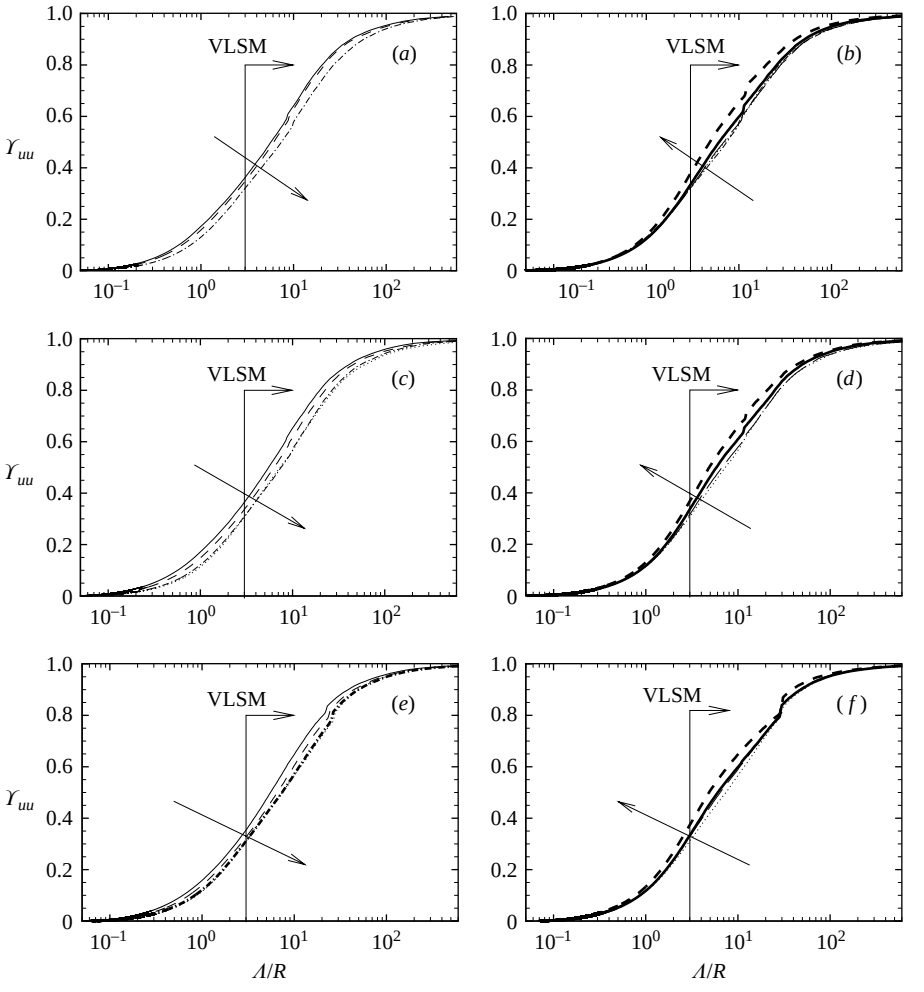

FIGURE 6. Cumulative streamwise kinetic energy fraction, Υ_{uu}, associated with structures with wavelengths less than Λ for $Re_\tau = 3815$ (a, b), $Re_\tau = 5884$ (c, d) and $Re_\tau = 7959$ (e, f). Lines are labelled as in figure 2(*a*).

to those found in Perry & Abell (1975) for comparable Reynolds numbers. While corrections could be applied to reduce these errors, their magnitudes do not affect any of the conclusions we shall make, and we prefer to present the data un-amended, with the proviso that, unlike the large scales, the contributions of the smallest scales must not be read from the cumulative plots because their small magnitude makes small errors significant.

Figure 6 presents the cumulative energy fraction of the streamwise velocity fluctuations as a function of wavelength and y-location. Irrespective of Reynolds number, more than 65 % of the energy is due to very large scales having wavelengths longer than $3R$ and more than 35 % of the energy is contained in wavelengths longer than $10R$. Thus, the very large scales play a surprisingly dominant role in the turbulence dynamics.

The distribution of the cumulative energy fraction, Υ_{uv}, with streamwise scale is presented in figure 7. Summarizing over all of the y-locations and Reynolds number,

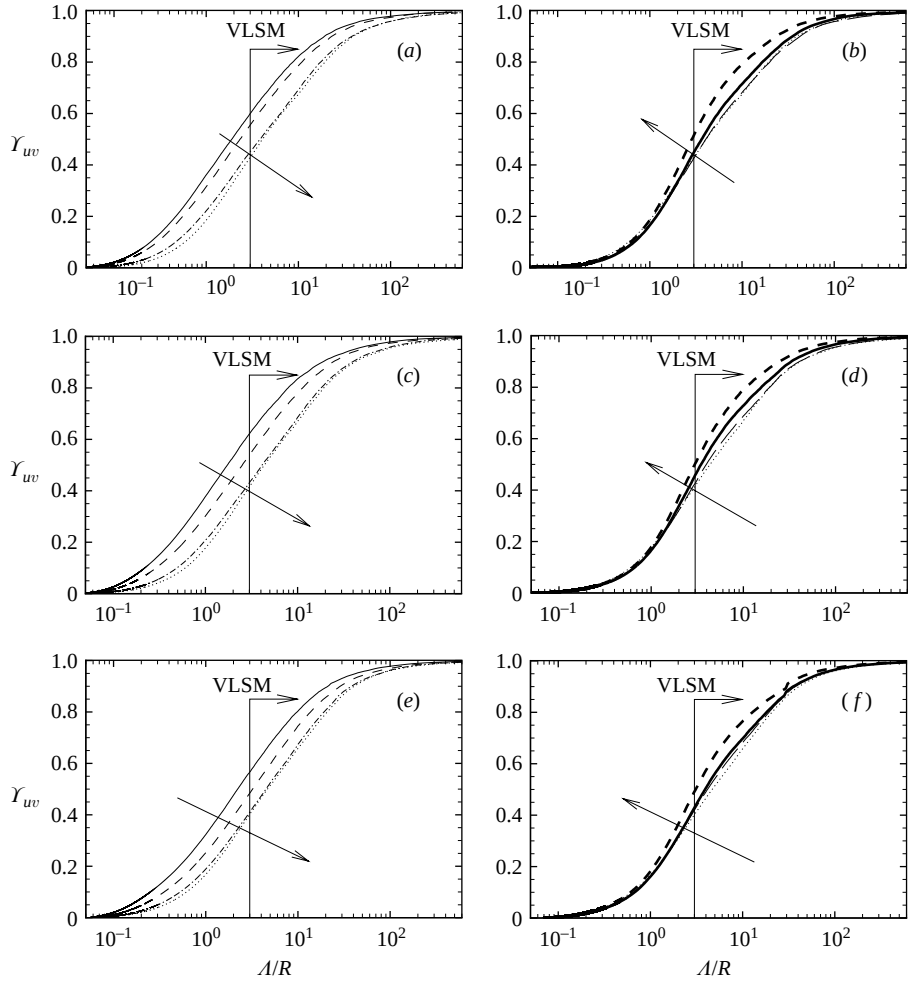

FIGURE 7. Cumulative Reynolds stress fraction, γ_{uv}, contained in scales with wavelength less than Λ/R for $Re_\tau = 3815$ (a,b), $Re_\tau = 5884$ (c,d) and $Re_\tau = 7959$ (e,f). Curves are labelled as in figure 2(*a*).

between 50 % and 60 % of the Reynolds shear stress comes from very-large-scale motions. This is much larger than expected if these motions were to be considered inactive in the logarithmic region. *Thus, the VLSMs are both energy containing and stress-active across the entire outer region.*

The streamwise wavelength that corresponds to half the cumulative streamwise energy, $(\Lambda/R)|_{\gamma=0.5}$, is presented in figure 8(*a*). Near the centreline of the pipe, half of the energy is contained in structures with wavelength greater than $3R$ (i.e. the VLSMs) and half is due to structures less than $3R$ in length (the LSMs and smaller). As the wall is approached, half the streamwise energy is contained in structures of increasing streamwise extent peaking at $7R$, and near the top of the logarithmic layer.

The streamwise scale that corresponds to half the cumulative contribution to the Reynolds shear stress, $(\Lambda/R)|_{\gamma=0.5}$ is presented in figure 8(*b*). Throughout most of the pipe's cross-section ($y/R > 0.1$), half of the Reynolds shear stress is due to structures with streamwise scale greater than $2R$. The trend closely emulates the behaviour of

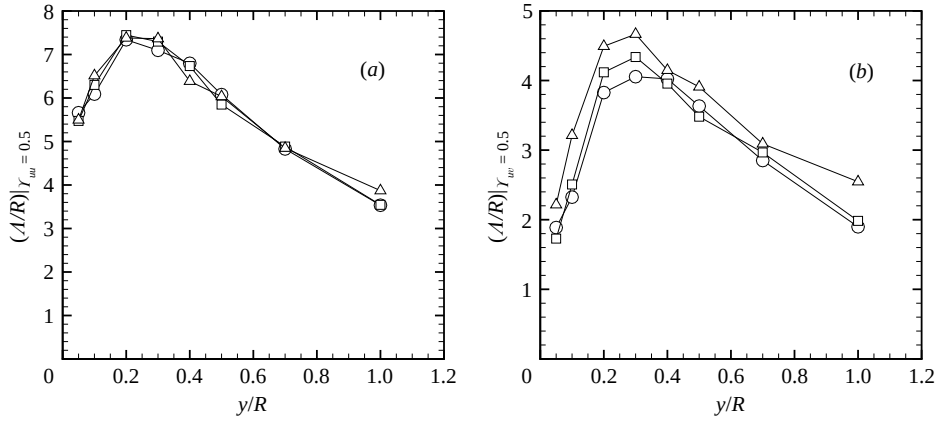

FIGURE 8. Streamwise scale that corresponds to half the cumulative energy, $(\Lambda/R)|_{\Upsilon=0.5}$, in Φ_{uu} (*a*) and to half the cumulative Reynolds stress, $(\Lambda/R)|_{\Upsilon=0.5}$, in Φ_{uv} (*b*), versus y. ($\bigcirc$, $Re_\tau = 3815$; $\square$, $Re_\tau = 5884$; $\triangle$, $Re_\tau = 7959$).

Υ_{uu}, figure 8(*a*). The largest structures contribute most significantly to Φ_{uv} between $y/R = 0.2$ and 0.3. The distribution of $(\Lambda/R)\,|_{\Upsilon=0.5}$ for Υ_{uv} suggests that near the wall, relatively small structures ($\Lambda \approx R$) are responsible for the majority of the Reynolds shear stress. Away from the wall, and in the logarithmic layer, larger structures with scales up to $5R$ are responsible for the majority of the Reynolds shear stress. This is the region of the flow where the Q2 ejections of the hairpins dominate over Q4 events (cf. Adrian, Meinhart & Tomkins 2000 and many earlier works on quadrant analysis).

5. Net force spectra

While turbulence research traditionally focuses on the mechanisms responsible for Reynolds shear stress, it is actually the y-derivative of $\overline{u'v'}$ that appears in the mean momentum equation for fully developed pipe and channel flow. It represents the net fictitious force exerted by the Reynolds shear stress. This force may or may not be significant when the underlying structures are themselves varying slowly in space, owing to their large size. In terms of the co-spectrum, the derivative is

$$\frac{\partial(-\overline{u'v'})}{\partial y} = \int_0^\infty \frac{\partial(-\Phi_{uv})}{\partial y}\,\mathrm{d}k_x, \tag{5.1}$$

showing that the derivative of Φ_{uv} represents the spectral contribution to the derivative of $\overline{u'v'}$. We refer to it as the net force spectrum or the derivative spectrum. The pre-multiplied derivative spectrum has been approximated by finite difference using the data available at the various y/R locations. The differencing introduces noise, and the values of Δy are not as small as they should be for accurate differencing, but the results in figure 9 are, revealing nonetheless.

First, with the exception of the spectrum for $y/R = 0.15$, the derivative is negative over the entire range of wavenumbers and y/R. These values of y all lie above the location of the maximum Reynolds shear stress at $y_p^+ = 2Re_\tau^{1/2}$ (Sreenivasan & Sahay 1997). Hence the y-derivative of $\overline{-u'v'}$ must be uniformly negative, representing a retardation of the mean velocity. This is consistent with the integrals of the curves in figure 9 being negative. Second, the derivative spectra possess two distinct ranges,

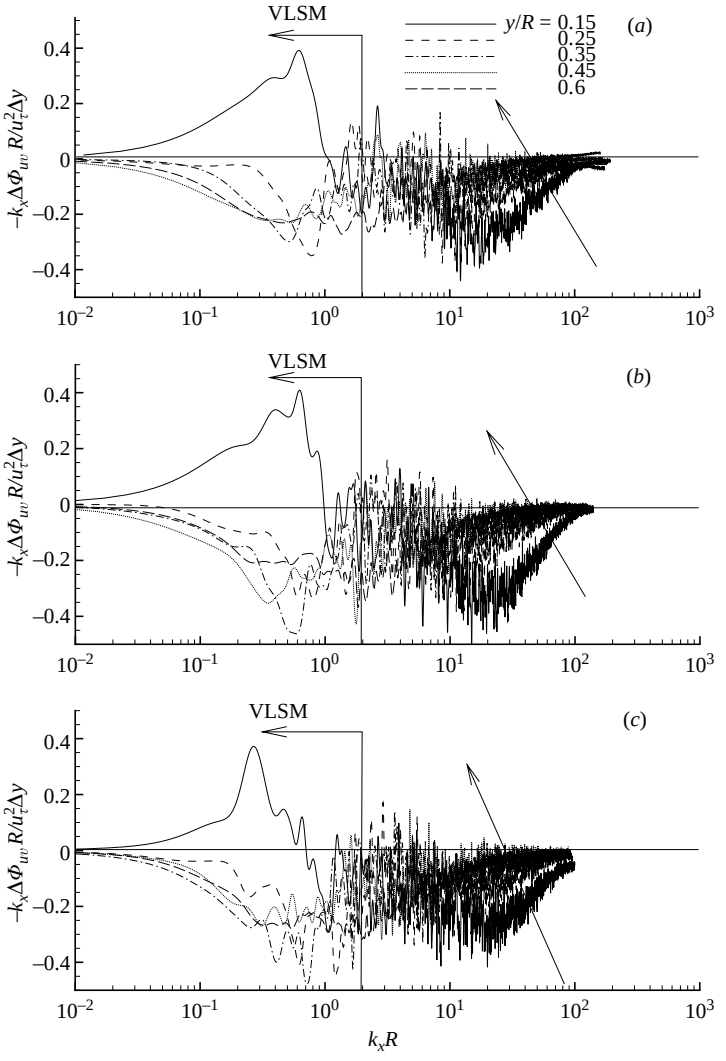

FIGURE 9. Vertical derivative of pre-multiplied co-spectra, Φ_{uv}, for $Re_\tau = 3815$ (*a*), $Re_\tau = 5884$ (*b*) and $Re_\tau = 7959$ (*c*). Note the positive peak in the low-wavenumbers region for $y/R = 0.15$.

each containing clear minima and separated by a maximum near $k_xR = 2 - 3$. This behaviour distinguishes the behaviour of the LSM and VLSM eddies even more prominently than the peaks in the uu-power spectrum. The contribution of the very-large-scale component is approximately equal to that of the LSM plus the main turbulent motion at the two highest Reynolds numbers and approximately half for the lowest Reynolds number. Thus, the VLSMs contribute very significantly to the net turbulent force that retards the mean velocity above the location of the maximum Reynolds shear stress. The contribution from the range of wavenumbers corresponding to the LSMs is relatively weak, while the contribution from the scales smaller than the LSMs is relatively strong.

The exceptional case in which the contribution of the derivative spectrum becomes positive occurs in the low-wavenumber range at $y/R = 0.15$. Since the u, v co-spectra

may be sensitive to effects of spatial resolution on the phase of the u- and v-signals (as opposed to the uu- or vv-spectra in which phase plays no role) we have not presented data below $y/R = 0.15$. Unfortunately, this does not allow us to explore the regions closer to the wall to see if this behaviour is characteristic throughout the logarithmic layer, or how it might change character on the other side of the maximum in $-\overline{u'v'}$. This would be a very interesting topic for future work. At y_p the area under the net force spectrum must vanish, so the spectrum must develop a region of positive area, and this appears to occur in the wavenumbers corresponding to the VLSMs. Below y_p the derivative-spectrum must become predominantly positive, representing acceleration of the flow. The positive values at $y/R = 0.15$ may be the first signs of this transition to near-wall inner-layer behaviour. It is well-known that the near-wall layer is accelerated by sweeps of high-momentum fluid. The net force spectra imply that an important part of these sweeps are these very-large-scale motions.

6. Discussion

As mentioned earlier, KA99 conjectured that the VLSMs consist of a concatenation of many bulges into a long train, such that the connections of the low-speed streaks from each bulge appear to be a much longer motion. From the lengths found above, each VLSM would consist of 2–8 bulges. This notion of building a long structure from shorter structures has its roots in the autogeneration mechanism by which one hairpin vortex creates another hairpin which creates another, and so on until a long packet of hairpins results (Smith *et al.* 1991; Zhou, Adrian & Balachandar 1996; Zhou *et al.* 1999; Adrian *et al.* 2000). The packets are prevalent in the logarithmic layer where their growth is consistent with a turbulence length scale proportional to y. There is evidence that the packets sometimes reach the outer edge of the boundary layer. The visualizations of Head & Bandyopadhyay (1981) indicate that at least some bulges are formed by a succession of hairpin vortices, and the mean velocity field of a bulge (Brown & Thomas 1977) is qualitatively consistent with fields created by the summation of many hairpins. Particle image velocimetry measurements (Adrian *et al.* 2000; Tomkins & Adrian 2003; Ganapathisubramani *et al.* 2005) support the picture of packets of hairpins creating long streaks of low-momentum fluid in the outer layer by lifting low-speed fluid upwards, in much the same way as the near-wall quasi-streamwise vortices form the near-wall low-speed streaks in the buffer layer. In essence, the concatenation of hairpins with trailing quasi-streamwise vortices forms what appears to be a long (but 'lumpy') set of quasi-streamwise vortices. Marusic (2001) shows how a model hairpin packet can account for the long tail of the longitudinal correlation function. The inclined heads of the hairpins also participate in the creation of low-momentum backflow, but since they are shorter than the legs of the hairpins they do not, on average, form connections between hairpins.

It is difficult to observe the very-large-scale motions by visualization or by PIV due to their great size. However, bulges are readily observed, and there is considerable evidence for the existence of multiple hairpin packets within bulges (cf. Adrian *et al.* 2000). Figure 10 presents an example of smoke wire visualization of pipe flow taken from the work of Lekakis (1988). The flow is left to right, and the smoke wire is location at $y/R = 0.021$. In the upper image, looking down on the (x, z)-plane, the smoke waivers sinuously with a wavelength somewhat greater than $2R$. It disperses before a longer wavelength can be observed. The side view in the middle image shows the smoke extending up to about $0.2R$ in the (x, y)-plane, e.g. filling the logarithmic layer. There are at least two regions, enclosed by boxes (a) and (b) that

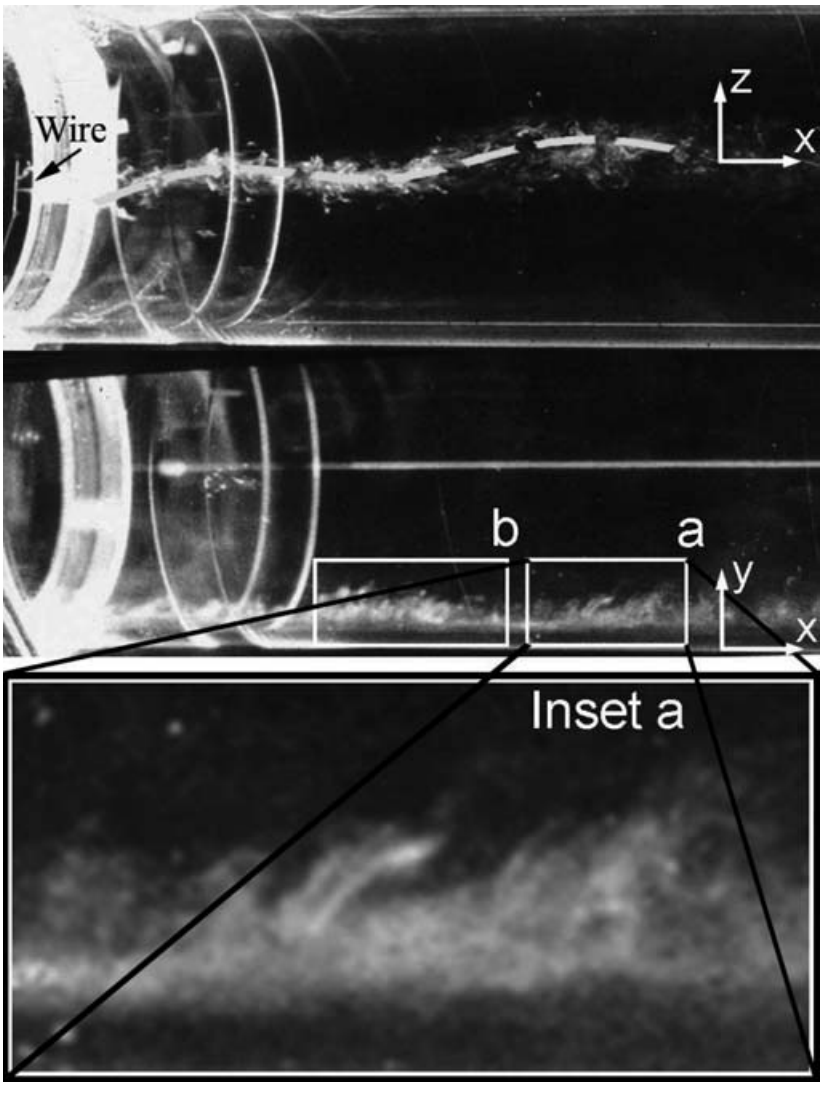

FIGURE 10. Smoke visualization in the streamwise–wall-normal (x, z)- and (x, y)-planes: note the large-scale oscillation of the turbulent bulge, consisting of smaller-scale structures aligned in the streamwise direction. Insets (*a*) and (*b*) enclose groups of inclined structures that may be a packets of hairpins. From Lekakis (1988).

contain patterns of groups of thin, 45° inclined structures consistent with the patterns expected from hairpins. Inspection of the top view of this flow and many other samples like it indicates that these patterns form along the wavering smoke streak. The picture is consistent with the smoke streak being a concatenation of hairpin packets. Time histories of the velocity support this picture. For example, the trace of $u(t)$ presented in KA99 shows the signature of hairpin packets riding atop the longer wave of the VLSM.

While the evidence suggests that hairpins concatenate to form packets, and packets concatenate to form LSMs, there are still no solid observations to prove or disprove the conjecture that bulges concatenate to form VLSMs. The possibility must be

left open that some mechanism other than packet dynamics may be at play. In fact, one interpretation of the significant difference between the scales of the VLSMs and the LSMs is that they result from different mechanisms. The interesting recent results on large-scale motions in transitional flow (Hof *et al.* 2004), and long, exact travelling wave solutions for low-Reynolds-number pipe flow (Wedin & Kerswell 2004; Priymak & Miyazaki 2004; Waleffe & Wang 2005) are intriguing in this regard. While the flows considered in those studies are still far removed from the high Reynolds numbers considered here, the possibility remains that such mechanisms or relatives of them can exist in the outer region. Even weak interaction with the packets could provide an agency to align them and thereby create long structures.

7. Summary and conclusions

Studies of large-scale and very-large-scale structures have been conducted in the outer region of fully developed turbulent pipe flow in the range of $192\,700 < Re_D < 422\,300$ (roughly $4000 < Re_\tau < 8000$). Pre-multiplied spectra of streamwise velocity fluctuations reveal very-large-scale energy-containing motions with mean wavelengths of up to $16R$ in the logarithmic region of pipe flow, and large-scale motions with mean wavelengths of $2R$–$3R$ throughout the layer. These results are consistent with those of KA99 and Jiménez (1998) for pipe flow and with del Alamo *et al.* (2004) for channels. The very-large-scale motions are not only energetic, but they also contribute a large fraction of the Reynolds shear stress, Typically, they contain half of the turbulent kinetic energy of the streamwise component and more than half of the Reynolds shear stress. Thus, they are both energetic and active. These results are consistent with the proper orthogonal decomposition analysis of channel flow by Liu *et al.* (2001), except that the limited streamwise extent of the latter study aliased the very-long-wavelength motions in a domain $2.4h$ long. The present study shows that much of the energy and the Reynolds shear stress attributed to the lowest-order POD modes in fact reside in the very-large-scale motions. Spectra of the y-derivatives of the Reynolds shear stress show that the very-large-scale motions contribute about the same amount to the net Reynolds shear force, $\mathrm{d}\overline{-u'v'}/\mathrm{d}y$, as the combination of all smaller motions, including the large-scale motions and the main turbulent motions. Although the main turbulent motions, defined nominally as those having wavelengths less than $0.2R$, contribute relatively little to the total Reynolds shear stress, they are important elements of the net Reynolds shear force. The clear spectral peak that characterizes the VLSMs suggests a periodic oscillation in the streamwise direction that is observed in flow visualization images, cf. figure 10. The images give clear evidence of the succession of inclined (presumably hairpin) vortices forming streaks. The oscillation of low-speed streaks formed by coherent alignment and induction may be the result of an instability similar to that described by Waleffe (1997), or it may be a consequence of the processes that create the alignment, similar to the way hairpins autogenerate to create alignment within packets. The length of the large-scale structures grows with distance from the wall at a rate that is roughly linear in the logarithmic layer, but slower in the wake region. Linear growth in the logarithmic layer is consistent with the relationship $\lambda_z^2 \propto y\lambda_x$ (del Alamo *et al.* 2004) if one assumes that $\lambda_z \propto y$, as found by Tomkins & Adrian (2003).

It is, perhaps, worthwhile to speculate on two possible ramifications of the dominant role played by the very large scales in wall turbulence. First, the very-large-scale motions are hardly local, and they are not therefore amenable to being represented

by gradient transport models. Following a suggestion in Hinze (1975) it would perhaps be better to separate the model of the total Reynolds stress into a small-scale component that is amenable to modelling with a gradient transport concept, and a very-large-scale component that cannot be statistically modelled because it is sensitive to boundary conditions and flow geometry. This component should be computed. Of course, large-eddy simulation does exactly this, but it might be possible to exploit the extremely large scale of the VLSMs to perform computations using unsteady three-dimensional Reynolds-averaged Navier–Stokes models with empirical transport coefficients suitably adjusted to remove the contribution of the VLSM.

Second, the very-large-scale motions may only exist in fully developed flows like pipe and channel flow or in slowly developing or equilibrium boundary layers. If the alignment mechanism is weak, and if the development is too fast or disturbed, long structures may not form. Without the alignment, coherent stress vanishes and the total stress may be altered, providing another reason to compute these motions instead of modeling them statistically.

This work was supported by the US National Science Foundation, Division of Atmospheric Sciences and the Leonard C. and Mary Lou Hoeft Endowment, University of Illinois. Funding from the ETH research commission under grant TH 15/04-2 is also acknowledged.

REFERENCES

Adrian, R. J., Meinhart, C. D. & Tomkins, C. D. 2000 Vortex organization in the outer region of the turbulent boundary layer. *J. Fluid Mech.* **422**, 1–54.

del Alamo, J. C., Jiménez, J., Zandonade, P. & Moser, R. D. 2004 Scaling of the energy spectra of turbulent channels. *J. Fluid Mech.* **500**, 135–144.

Bandyopadhyay, P. 1982 Period between bursting in turbulent boundary layers. *Phys. Fluids* **25**, 1751–1754.

Bendat, J. S. & Piersol, A. G. 1986 *Random Data: Analysis and Measurement Procedures.* John Wiley & Sons.

Blackwelder, R. F. & Kovasznay, L. S. G. 1972 Time scales and correlations in a turbulent boundary layer. *Phys. Fluids* **15**, 1545.

Bradshaw, P. 1967 'Inactive' motion and pressure fluctuations in turbulent boundary layers. *J. Fluid Mech.* **30**, 241–258.

Brown, G. L. & Thomas, A. S. W. 1977 Large structure in a turbulent boundary layer. *Phys. Fluids* **20**, S243.

Bullock, K. J., Cooper, R. E. & Abernathy, F. H. 1978 Structural similarity in radial correlations and spectra of longitudinal velocity fluctuations in pipe flow. *J. Fluid Mech.* **88**, 585–608.

Cantwell, B. J. 1981 Organized motion in turbulent flow. *Annu. Rev. Fluid Mech.* **13**, 457–515.

Falco, R. E. 1991 A coherent structure model of the turbulent boundary-layer and its ability to predict reynolds number dependence. *Phil. Trans. R. Soc. Lond.* A **336**, 103–129.

Favre, A. J., Gaviglio, J. J. & Dumas, R. 1967 Structure of velocity space-time correlations in a boundary layer. *Phys. Fluids* **10**, S138–S145.

Fleischmann, S. T. & Wallace, J. M. 1984 Mean streamwise spacing of organized structures in transitional and developed bounded flows. *Exps. Fluids* **22**, 766–768.

Ganapathisubramani, B., Hutchins, N. L., Hambleton, W. T., Longmire, E. K. & Marusic, I. 2005 Investigation of large-scale coherence in a turbulent boundary layer using two-point correlations. *J. Fluid Mech.* **524**, 57–80.

Grant, H. L. 1958 The large eddies of turbulent motion. *J. Fluid Mech.* **4**, 149–190.

Head, M. R. & Bandyopadhyay, P. 1981 New aspects of turbulent boundary layer structure. *J. Fluid Mech.* **107**, 297–338.

Hinze, J. O. 1975 *Turbulence*. McGraw-Hill.

Hites, M. H. 1997 Scaling of high-Reynolds number turbulent boundary layers in the national diagnostic facility. PhD thesis, Illinois Institute of Technology.

Hof, B., Doorne, C. W. H., Westerweel, J., Nieuwstadt, F. T. M., Faisst, H., Eckhardt, B., Wedin, H., Kerswell, R. R. & Waleffe, F. 2004 Experimental observation of nonlinear traveling waves in turbulent pipe flow. *Science* **305**, 1594–1598.

Hommema, S. E. 2001 Very-large scale motions in wall-bounded turbulent flows. PhD thesis, Department of Theoretical and Applied Mechanics, Univeristy of Illinois at Urbana-Champaign.

Hunt, J. C. R. & Morrison, J. 2000 Eddy structure in turbulent boundary layers. *Eur. J. Mech.* B **19**, 673–694.

Jiménez, J. 1998 The largest scales of turbulent wall flows. *Center for Turbulence Research, Annual Research Briefs*, pp. 137–154. Standford University.

Jiménez, J., del Alamo, J. C. & Flores, O. 2004 The large scale dynamics of near-wall turbulence. *J. Fluid Mech.* **505**, 179–199.

Kim, K. C. & Adrian, R. J. 1999 Very large-scale motion in the outer layer. *Phys. Fluids* **11**, 417–422 (referred to herein as KA99).

Kovasznay, L. S. G., Kibens, V. & Blackwelder, R. F. 1970 Large-scale motion in the intermittent region of a turbulent boundary layer. *J. Fluid Mech.* **41**, 283–325.

Krogstad, P. A., Antonia, R. A. & Browne, L. W. B. 1992 Comparison between rough- and smooth-wall turbulent boundary layers. *J. Fluid Mech.* **245**, 599–617.

Laufer, J. & Narayanan, M. A. B. 1971 Mean period of the turbulent producion mechanism in a boundary layer. *Phys. Fluids* **14**, 182–183.

Lawn, C. J. 1971 The determination of the rate of dissipation in turbulent pipe flow. *J. Fluid Mech.* **48**, 477–505.

Lekakis, I. O. 1988 Coherent structures in fully developed pipe flow. PhD thesis, Department of Mechanical Engineering, University of Illinois at Urbana-Champaign.

Liu, Z.-C., Adrian, R. J. & Hanratty, T. J. 2001 Large-scale modes of turbulent channel flow: transport and structure. *J. Fluid Mech.* **448**, 53–80.

Marusic, I. 2001 On the role of large-scale structures in wall turbulence. *Phys. Fluids* **13**, 735–743.

Morrison, J. F., McKeon, B. J., Jiang, W. & Smits, A. 2004 Scaling of the streamwise velocity component in turbulent pipe flow. *J. Fluid Mech.* **508**, 99–131.

Murlis, J., Tsai, H. M. & Bradshaw, P. 1982 The structure of turbulent boundary layers at low Reynolds numbers. *J. Fluid Mech.* **122**, 13–56.

Perry, A. E. & Abell, C. J. 1975 Scaling laws for pipe-flow turbulence. *J. Fluid Mech.* **67**, 257–271.

Perry, A. E., Henbest, S. & Chong, M. S. 1986 A theoretical and experimental study of wall turbulence. *J. Fluid Mech.* **165**, 163–199.

Priymak, V. G. & Miyazaki, T. 1994 Long-wave motions in turbulent shear flows. *Phys. Fluids* **6**, 3454–3464.

Priymak, V. G. & Miyazaki, T. 2004 Direct numerical simulation of equilibrium spatially localized structures in pipe flow. *Phys. Fluids* **16**, 4221–4234.

Smith, C. R., Walker, J. D. A., Haidari, A. H. & Sobrun, U. 1991 On the dynamics of near-wall turbulence. *Phil. Trans. R. Soc. Lond.* A **336**, 131–175.

Sreenivasan, K. R. & Sahay, A. 1997 The persistence of viscous effect in the overlap region and the mean velocity in turbulent pipe and channel flow. In *Self Sustaining Mechanisms of Wall Turbulence* (ed. R. Panton), vol. 15. WIT Press, Bath, UK.

Tomkins, C. D. & Adrian, R. J. 2003 Spanwise structure and scale growth in turbulent boundary layers. *J. Fluid Mech.* **490**, 37–74.

Townsend, A. A. 1958 The turbulent boundary layer. In *Boundary Layer Research* (ed. H. Görtler), vol. 1. Springer.

Townsend, A. A. 1961 Equilibrium layers and wall turbulence. *J. Fluid Mech.* **11**, 97–120.

Townsend, A. A. 1976 *The Structure of Turbulent Shear Flow*, 2nd edn. Cambridge University Press.

Tritton, D. J. 1967 Some new correlation measurements in a turbulent boundary layer. *J. Fluid Mech.* **28**, 439–462.

Waleffe, F. 1997 On a self-sustaining process in shear flows. *Phys. Fluids* **9**, 883–900.

Waleffe, F. & Wang, J. 2005 transition threshold and self sustaining process. In *IUTAM Symposium on Laminar-Turbulent Transition and Finite Amplitude Solutions* (ed. T. Mullin). Springer.

Wedin, H. & Kerswell, R. R. 2004 Exact coherent structures in pipe flow: travelling wave solutions. *J. Fluid Mech.* **508**, 333–371.

Zhou, J., Adrian, R. J. & Balachandar, S. 1996 Auto-generation of near wall vortical structure in channel flow. *Phys. Fluids* **8**, 288.

Zhou, J., Adrian, R. J., Balachandar, S. & Kendall, T. 1999 Mechanisms for generating coherent packets of hairpin vortices in channel flow. *J. Fluid Mech.* **387**, 353–396.